Structural and magnetic characterization of Sm³⁺ ion substituted Zn-Mn nanoferrites synthesized by glycol-thermal method

T. A. Nhlapo[1], J. Z. Msomi[2], T. Moyo[3]
[1]Department of Medical Physics, Sefako Makgatho Health Sciences University, P. O. Box 146, Medunsa 0204, South Africa.
[2]Department of Physics & Engineering, University of Zululand, Private Bag X1001, KwaDlangezwa 3886, South Africa.
[3]School of Chemistry and Physics, University of KwaZulu-Natal, Private Bag X54001, Durban 4000, South Africa

E-mail address: amos.nhlapo@smu.ac.za

Abstract. The magnetic properties of $Zn_{0.5}Mn_{0.5}Sm_xFe_{2-x}O_4$ ($0 \leq x \leq 0.05$) nanosized produced by glycol thermal methods. Crystallite size in the range 12-17 nm were investigated. XRD analysis confirmed a single phase cubic spinel structure in all the compounds investigated. The elemental composition was confirmed by EDX analysis and microstructure were examined by TEM and SEM measurements. TEM and SEM images showed nearly spherical particles with uniform particle size distributions. The Mössbauer spectra of $Zn_{0.5}Mn_{0.5}Fe_2O_4$ ($x = 0$) oxide could be resolved into two quadrupole doublets indicative of paramagnetic spin state. Sm³⁺ substituted $Zn_{0.5}Mn_{0.5}Sm_xFe_{2-x}O_4$ ($0.01 \leq x \leq 0.05$) fine powders show weak sextets in addition to broad doublets attributed some particles' magnetic moments in an ordered magnetic phase. The compounds have small coercive fields and high saturation magnetization (40 emu/g to 60 emu/g) which reduces with increasing Sm³⁺ content due to the paramagnetic nature of Sm ions. Results show that $Zn_{0.5}Mn_{0.5}Sm_xFe_{2-x}O_4$ substituted Sm are suitable for applications in electronic devices requiring high frequencies.

1. Introduction

Nano crystalline ferrites are a group of magnetic nanoparticles with the general chemical formula MFe_2O_4 where M are divalent ions such as Zn^{2+}, Cd^{2+}, Co^{2+}, Mn^{2+} etc. or a mixture. Their properties such as chemical stability at high temperature, high dc resistivity, mechanical hardness, high Curie temperature, and high permeability make them good materials for technology and industry [1]. Zn substituted Mn ferrites have low resistivity, high power loses making them suitable for applications in electronic devices such as transformers, inductor cores, converters, magnetic heads and electromagnetic wave absorbers [2, 3]. Substitution by low concentrations of rare earth ions can improve the ferrite properties [4, 5]. V. J. Angadi et al [4] prepared $Zn_{0.5}Mn_{0.5}Sm_xFe_{2-x}O_4$ ($0 \leq x \leq 0.05$) by combustion method and carried out Mössbauer spectral studies. Sm³⁺ doped Zn-Mn ferrites were found to have potential applications in electronic devices requiring high frequency [4]. The room temperature Mössbauer spectra of the $Zn_{0.5}Mn_{0.5}Sm_xFe_{2-x}O_4$ ($0 \leq x \leq 0.05$) compounds were indicative of paramagnetic spin phase [4].

La ions were found to have preference for octahedral (B) sites in Ni-Zn ferrites produced by sol-gel method [5]. The distribution of metal cations in A and B sites is sensitive to the sample preparation method and can affect the properties [6]. Magnetization data can reveal additional information such as superparamagnetism which cannot be clearly observed from only Mössbauer studies. However, no studies were done on the low temperature hysteresis loops for these compounds. The information deduced from *M (H)* curves will provide more understanding of the magnetic behaviour of these compounds at low temperature.

In this study we aim to synthesize materials suitable for high frequency electronic devices. Moreover to investigate the effect of Sm $^{3+}$ ion substitution on structural and temperature-dependent magnetic properties of $Zn_{0.5}Mn_{0.5}Sm_xFe_{2-x}O_4$ ($0 \leq x \leq 0.05$) ferrite nano materials produced by glycol-thermal process. To achieve this, the study was done using several techniques such as XRD, TEM, SEM, EDX and Mössbauer spectroscopy, VSM and a mini- cryogenic free system.
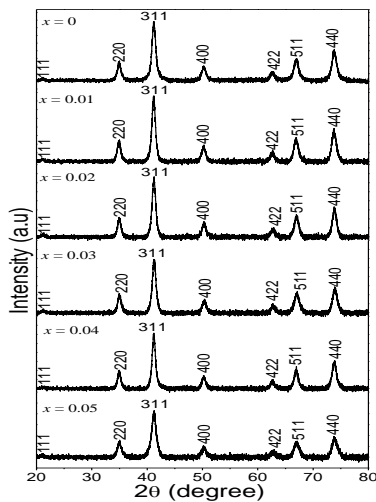
2. Experimental details

Materials used to synthesize nano crystalline $Zn_{0.5}Mn_{0.5}Sm_xFe_{2-x}O_4$ ($0 \leq x \leq 0.05$) were of high purity (98+) and supplied by Aldrich Sigma Company of South Africa. The samples were prepared by glycol-thermal process from metal chlorides $FeCl_3 \cdot 6H_2O$, $MnCl_2 \cdot 6H_2O$, $SmCl_3 \cdot 6H_2O$ and $ZnCl_2$ following procedures reported previously [7]. The XRD analysis was done by using a monochromatic beam of Co K_α radiation ($\lambda = 1.7903$ Å) on a model PANalytical Empyrean diffractometer. The morphology and micro-structure were investigated on a high-resolution scanning electron microscope (HRSEM, Ultra Plus ZEISS-FEG HRSEM instrument) and high resolution transmission electron microscope (HRTEM, type: Jeol_JEM-1010), respectively. The Mössbauer spectra were recorded at about 300 K using a conventional constant acceleration Mössbauer spectrometer with a ^{57}Co source sealed in Rh matrix. The room temperature magnetization measurements were performed by using a Lake-Shore model 735 vibrating sample magnetometer and temperature-dependent magnetization measurements were performed by Cryogenic Ltd mini-cryogen free system from 2 – 300 K.

3. esults and discussions

The XRD patterns for the as-synthesized $Zn_{0.5}Mn_{0.5}Sm_xFe_{2-x}O_4$ ($0 \leq x \leq 0.05$) fine powders are shown in figure 1. The XRD patterns of all samples exhibit typical reflections of (111), (220), (311), (400), (422), (511) and (440) planes of a cubic spinel lattice with no traces of impurity phases. The broad peaks observed are indicative of fine particles. The average crystallite sizes listed in Table 1 were computed from the most intense (311) XRD peak using the Debye Scherer formula [8]. The reaction pressure has an efficient effect on crystallite sizes. The crystallite size fluctuates between 12 nm and 17 nm. The fluctuation is caused by reaction pressure during sample preparation process. It is observed from the table that a higher reaction pressure results in a higher particles size and vice versa. A typical TEM image is shown in Figure 2 for the sample $x = 0.05$. The particles are nearly spherical in shape with average particle diameter of about 15 nm, comparable to about 13 nm estimated from XRD data. The distributions of particle sizes are shown in Figures 3 sample $x = 0.05$ show narrow particle size distributions. The typical SEM image for sample $x = 0.05$ shown in Figure 4 (a) which also reveal nearly spherical agglomerated fine particles with homogeneous surface morphology. The elemental composition was confirmed by EDX shown in Figure 4 (b) and reveals the presence of characteristics peaks of Mn, Zn, Fe and Sm for $x = 0.05$ sample.
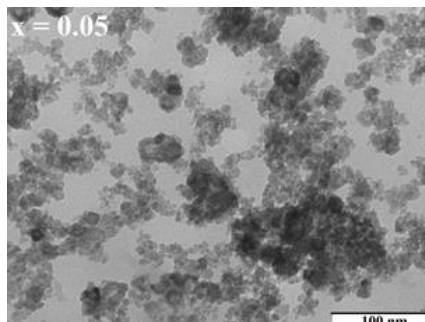
The Mössbauer spectra for $Zn_{0.5}Mn_{0.5}Sm_xFe_{2-x}O_4$ nanosized oxides are shown in Figure 5. The best fit to the experimental data for the compound $Zn_{0.5}Mn_{0.5}Fe_2O_4$ ($x = 0$) was obtained with two doublets associated with paramagnetic spin state. The Mössbauer spectra of Sm substituted Zn-Mn in the current work show weak sextets which were not observed in same compounds produced by combustion method [4]. This shows the effect of sample preparation method on the magnetic properties. The weak sextets (2-22 %) may be due to single domain particles with ordered magnetic phase and the redistribution of cations in tetrahedral (A) or octahedral (B). The fine powders of $Zn_{0.5}Mn_{0.5}Sm_xFe_{2-x}O_4$ ($0.01 \leq x \leq 0.05$) could be fitted with two sextets and two quadrupole doublets associated with ^{57}Fe nuclei distributed

Figure 1. XRD patterns for as-prepared $Zn_{0.5}Mn_{0.5}Sm_xFe_{2-x}O_4$ oxides.

Table 1. Crystallite size (*D*), reaction pressures (P), lattice parameter (*a*) and X-ray density (ρ) for $Zn_{0.5}Mn_{0.5}Sm_xFe_{2-x}O_4$ oxides as function.

x	D_{XRD} (nm) ± 0.2	*P* (psi)	*a* (Å) ±0.001	ρ (g/cm^3) ±0.003
0.00	14.7	90	8.439	5.213
0.01	15.1	80	8.440	5.223
0.02	14.4	40	8.435	5.262
0.03	14.0	30	8.425	5.302
0.04	16.5	60	8.436	5.268
0.05	12.5	20	8.430	5.336

within A and B sites. The spectrum for sample *x* = 0.04 with larger particles (~17 nm) that resulted from reaction highest pressure, shows stronger sextets (~42 %) due to ferromagnetic ordering large particles. The average isomer shift was about 0.35 mm/s for the whole composition range. The s electron charge distribution of Fe ions was therefore weakly affected by Sm ion substitution. The A site quadrupole splitting and line width were generally lower compared to B sites. This behaviour is attributed to high symmetry at A site.
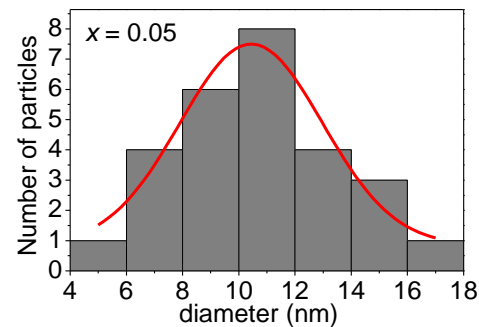
The typical room temperature magnetization curves are presented in Figure 6 for *x* = 0, *x* = 0.03 and *x* = 0.05 oxides. The insert shows the magnified view at low magnetic field. $Zn_{0.5}Mn_{0.5}Sm_xFe_{2-x}O_4$ (0.01≤ *x* ≤ 0.05) samples have small coercive fields and high saturation magnetization which are relevant microwave properties [8]. Very small coercive magnetic fields and remnant magnetization are indicative of superparamagnetic nanoparticles [9]. Saturation magnetization values can be computed by fitting initial magnetization curves with the empirical law of approach to saturation based on the relation $M_S(H) = M_S(0)(1-a/H-b/h^2) + \chi H$ [10, 11], where *a* and *b* are the fitting parameters and χ is the high-field susceptibility due to field induced band splitting and are shown in Figure 7. Magnetization reduces from 58.9 emu/g at *x* = 0 to 47.2 emu/g at *x* = 0.05, with increasing Sm^{3+} ion content. This can be explained by the weakening of the super-exchange interactions between the B sites magnetic moments due to substitution of Fe^{3+} ions by paramagnetic Sm^{3+} ions. The magnitude of the magnetization in ferrites is
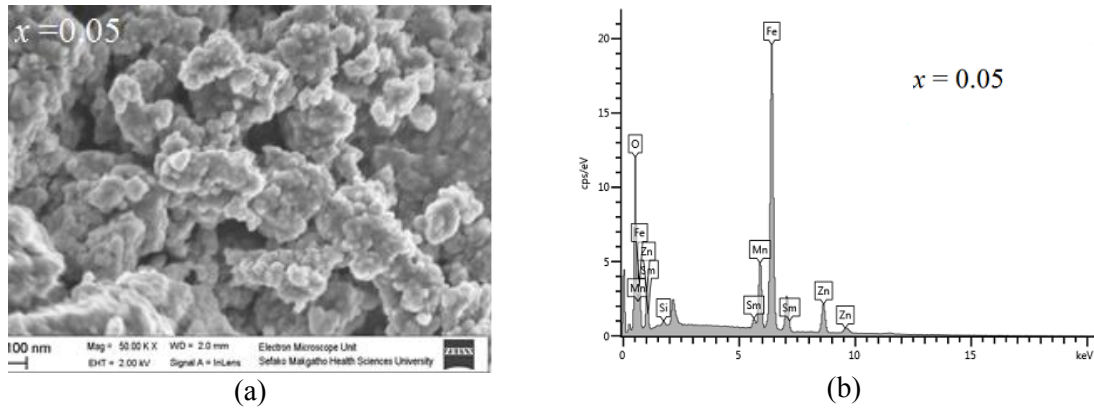

Figure 2. TEM image for as-prepared $Zn_{0.5}Mn_{0.5}Sm_{0.05}Fe_{1.95}O_4$ (*x* = 0.05).

Figure 3. Particle size distribution for as-prepared $Zn_{0.5}Mn_{0.5}Sm_{0.05}Fe_{1.95}O_4$ (*x*=0.05).

**Figure 4.** SEM image (a) and EDX image (b) for $Zn_{0.5}Mn_{0.5}Sm_{0.05}Fe_{1.95}O_4$ ($x = 0.05$).

due to the difference between the magnetization at A- and B sub-lattices ($M = |M_B - M_A|$) [12]. For the $Zn_{0.5}Mn_{0.5}Fe_2O_4$ ($x = 0$) oxide magnetization is due to the magnetic Mn and Fe ions in A and B sites. Dilution of the B site magnetic neighbors by paramagnetic Sm^{3+} ions causes weaker super-exchange interactions between magnetic moments (B-O-B) and thus low B site magnetization (M_B). These results are well in agreement with Mössbauer results. The values of the magnetic moment per formula unit (magneton number) were calculated using the relation $\eta_B = MM_S/5585$ [11]. Where M is the molecular weight of the ample and M_s is the saturation magnetization. A general decrease in η_B relates well with reduction in saturation magnetization observed with increasing concentration of Sm^{3+} ions. This can be explained by the Neel's theory of ferrimagnetism [13] due to the nonmagnetic nature of Sm ions.
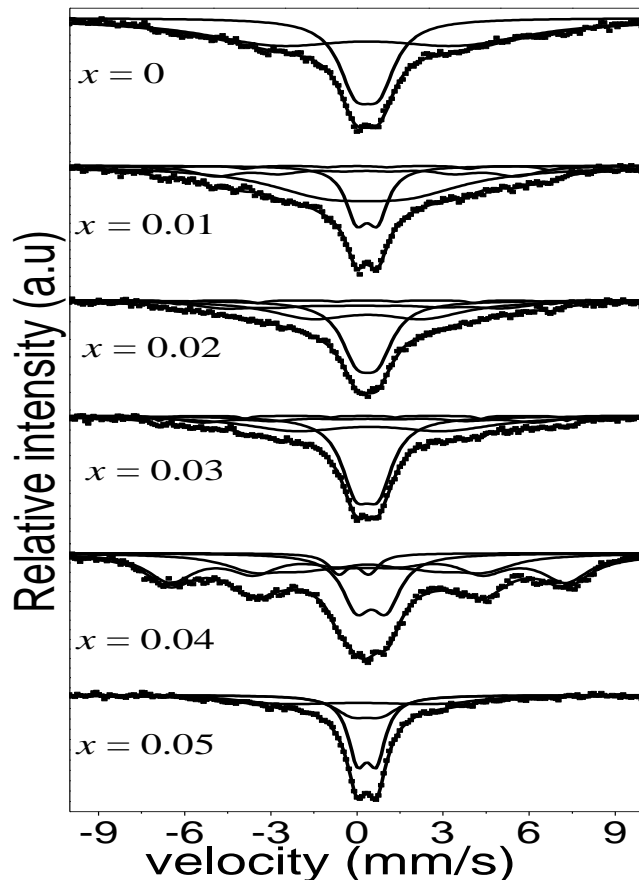
Figure 5. Room temperature Mössbauer spectra for the as-prepared $Zn_{0.5}Mn_{0.5}Sm_xFe_{2-x}O_4$ oxides indicating paramagnetic nature of compounds.
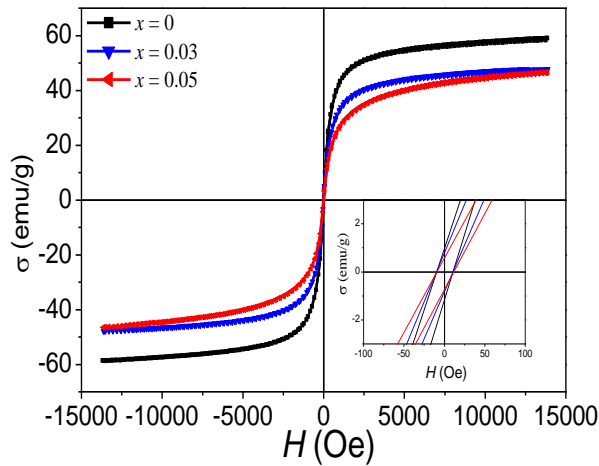
**Figure 6.** Room temperature hysteresis loops for $Zn_{0.5}Mn_{0.5}Sm_xFe_{2-x}O_4$ oxides.
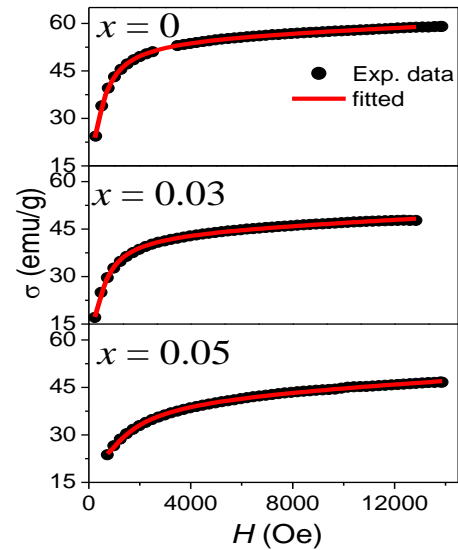
Figure 7. Initial magnetization with best fit curves based on empirical law approach to saturation magnetization.

The ratios of remnant (M_R) to saturation magnetizations (M_S) are listed in Table 2. M_R/M_S ratio is called the squareness of a hysteresis loop. It was about 2 % for samples $Zn_{0.5}Mn_{0.5}Sm_xFe_{2-x}O_4$ ($0.01 \leq x \leq 0.04$). An increase to about 5 % has been observed for sample $x = 0.05$. Small squareness is associated with non-interacting single domain particles [14]. The smaller values observed in the current study are in agreement with the Mossbauer data which shows paramagnetic spin state in the $Zn_{0.5}Mn_{0.5}Sm_xFe_{2-x}O_4$ ($0 \leq x \leq 0.05$) fine powders. The typical hysteresis loops recorded at different isothermal temperature from 2 K - 300 K to 2 k are shown in Figure 8 for sample $x = 0.05$. Small coercive fields are observed even at low temperatures. Magnetization increases with reducing temperature due to spin freezing of the magnetic moments [15]. Small coercive fields are observed for these samples even at lower temperatures. A plot of the variation of the magnetization for different compositions with increasing temperature is also shown in Figure 9. Reduction in magnetization with increasing temperature is due to increasing thermal energies resulting in disordered magnetic spin phase.

Table 2. Room temperature magnetization parameters (deduced from Figure 7) and magneton number (η_B) for $Zn_{0.5}Mn_{0.5}Sm_xFe_{2-x}O_4$ oxides.

X	M_r (emu/g)	M_s (emu/g)	SQR	μ_B (emu/g)
0	1.082	58.9	0.0184	2.49
0.03	0.808	44.6	0.0169	1.91
0.05	0.651	42.7	0.0525	1.84
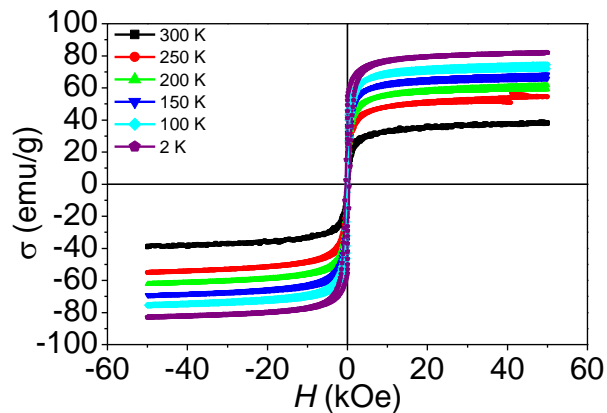
Figure 8. Temperature-dependent magnetization curves for $Zn_{0.5}Mn_{0.5}Sm_{0.05}Fe_{1.95}O_4$ oxide.
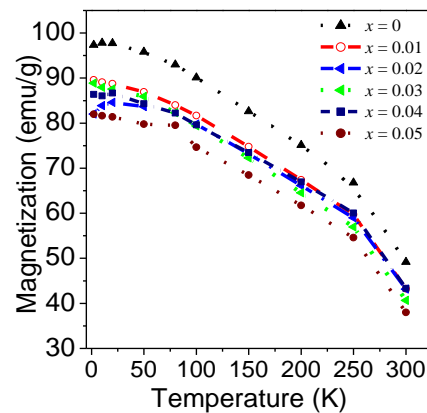
Figure 9. Highest magnetizations deduced from different isothermal temperatures.

4. Conclusions

Nanostructured $Zn_{0.5}Mn_{0.5}Sm_xFe_{2-x}O_4$ ($0 \leq x \leq 0.05$) were successfully prepared by glycol thermal technique. Synthesis route have significant effect on the structural and magnetic properties. Room temperature Mössbauer spectra of the samples investigated in the current study show weak sextet superimposed with paramagnetic doublets. Magnetization data revealed superparamagnetic nature of the compounds investigated. Slight change in coercive fields are observed at lower measuring temperatures. A reduction in saturation magnetization with increasing Sm content associated with the paramagnetic nature of Sm^{3+} ion has been observed. These properties make the compounds suitable for high frequency applications.

References
[1]   S. Hcni, N. Kouki, A. Omri, A. Dhahri, M. L. Bouazizi, J. Magn. Magn. Mater. 464 (2018) 91.
[2]   W.R. Agami J. Phys. Condens. Mater. 534 (2018) 17.
[3]   Md. D. Rahaman, Md. D. Dalim Mia, M.N.I. Khan, A.K.M A. Hossain, J. Magn. Magn. Mater. 404 (2016) 238.
[4]   V. J. Angadia, S. P. Kubrin, D. A. Sarychev, S. Matteppanavar, B. Rudraswamy, H. Liu, K. Praveena, J. Magn. Magn. Mater. 441 (2017) 348.
[5]   Y. Wang, X Wu, W. Zhang, W. Chen, J. Magn. Magn. Mater. 398 (2016) 90.
[6]   J. Hua, Y. Liu, L. Wang, M. Feng, J. Zhao, H. Li, J. Magn. Magn. Mater. 402 (2016) 166.
[7]   J. Z. Msomi, Nhlapo T. A, T. Moyo; J. Snyman, A. M. Strydom, J. Magn. Magn. Mater. 373 (2015) 74.
[8]   I. Sadiq, S.Naseem, M. N. Ashiq, M. A. Iqbal, I. Ali, J. Magn. Magn.Mater. 395 (2015) 159.
[9]   J. Wang, X. Shao, G. Tian, Z. Li, W. Bao, J. Mater. Lett. 192 (2017) 36.
[10]   P. T. Phuong, P. H. Nam, D. H. Man, In-Jab Lee J. Magn. Magn. Mater. 433 (2017) 76.
[11]   J. M. D. Coey, Magnetism and Magnetic Materials, Cambridge University press, UK, 2010, pp. 218-244.
[12]   M. Gupta, Anu, R. K. Mudsainiyan, B. S Randhawa J. Analyt Appl. Pyrol. 116 (2015) 75.
[13]   M. Gupta, B.S. Randhawa, J. Alloys Compd. 626 (2015) 421.
[14]   A. V. Raut, D. V. Kurmude, D. R. Shangule, K. M. Jadhav, Mater. Res. Bull. 63 (2015) 123.
[15]   P. Masina, T. Moyo, H. M. I. Abdallah J. Magn. Magn. Mater. 381 (2015) 41.